



Dalton
Transactions

**Solid-State and Solution-Phase Characterization of Sm^{II}-
Aza[2.2.2]cryptate and Its Methylated Analogue**

Journal:	<i>Dalton Transactions</i>
Manuscript ID	DT-COM-06-2022-001823
Article Type:	Communication
Date Submitted by the Author:	09-Jun-2022
Complete List of Authors:	Bokouende, Sergely Steephen; Wayne State University Jenks, Tyler; Wayne State University Ward, Cassandra; Wayne State University Allen, Matthew; Wayne State University, Chemistry

SCHOLARONE™
Manuscripts

COMMUNICATION

Solid-State and Solution-Phase Characterization of Sm^{II}-Aza[2.2.2]cryptate and Its Methylated Analogue

Sergely Steephen Bokouende,^a Tyler C. Jenks,^a Cassandra L. Ward,^b and Matthew J. Allen^{*,a}

Received 00th January 20xx,
Accepted 00th January 20xx

DOI: 10.1039/x0xx00000x

Two new Sm^{II}-azacryptates are reported that differ in steric hindrance and Lewis basicity of donor atoms. The sterically hindered complex has a smaller coordination number and a more negative electrochemical potential than the complex with less steric hindrance.

Complexes of divalent lanthanide (Ln^{II}) ions have attracted attention in recent years owing to their interesting luminescence, magnetic, and electrochemical properties.^{1–25} One such group of Ln^{II} complexes that have been the subject of extensive investigation with regard to their structural, photophysical, and electrochemical properties is the Ln^{II}-cryptates.^{2,26–42} In many studies, cryptands such as 4,7,13,16,21,24-hexaoxa-1,10-diazabicyclo[8.8.8]hexacosane (**222**) and 5,6-benzo-4,7,13,16,21,24-hexaoxa-1,10-diazabicyclo[8.8.8]hexacos-5-ene are used to encapsulate Ln^{II} ions,^{26–32,37–42} and reported Ln^{II}-cryptates have luminescence and electrochemical properties that are useful in applications including light-emitting diodes, imaging, and catalysis.^{2,35,43} The luminescence and electrochemical properties of Ln^{II}-cryptates are dependent on both the Ln^{II} ion and the type of donor atoms in the cryptand.^{28,42} As such, it is critical to study the impact of donor atoms on the structural, spectroscopic, and electrochemical properties of Ln^{II}-cryptates. To address this need, the impact of strong Lewis base donors (amines) on the properties of Ln^{II} cryptates has been investigated with divalent europium and ytterbium^{2,28,32,34–36} using two nitrogen containing azacryptands: 1,4,7,13,16,21,24-octazabicyclo[8.8.8]hexacosane (**1**) and 4,7,13,16,21,24-hexamethyl-1,4,7,13,16,21,24-octazabicyclo[8.8.8]hexacosane (**2**).^{2,28,32–36} However, reports

to date with azacryptates have focused only on complexes of Eu^{II} and Yb^{II}. To enable the study of periodic trends relative to bonding in divalent lanthanides, the study of ligands **1** and **2** with Sm^{II} is a critical next step because Sm^{II} has the most positive electrochemical potential after Eu^{II} and Yb^{II}. Acquiring structural, spectroscopic, and electrochemical data of Sm^{II}-cryptates with cryptands **1** and **2** is expected to aid in the design of new cryptands and other macrocyclic ligands for Ln^{II} ions. Herein, we present solid-state characterization of [Sm^{II}]**1** and [Sm^{II}]**2** and compare trends in bonding with previously reported [Eu^{II}]**1**, [Yb^{II}]**1**, [Eu^{II}]**2**, and [Yb^{II}]**2**.^{28,34} We also report spectroscopic studies of [Sm^{II}]**1** and [Sm^{II}]**2** in acetonitrile and *N,N*-dimethylformamide and the electrochemical potentials of the two complexes in *N,N*-dimethylformamide.

We sought to obtain structural information of Sm^{II}-cryptates to compare trends in bonding with reported Eu^{II}- and Yb^{II}-containing cryptates of cryptands **1** and **2**.^{28,34} Reaction of SmI₂ with **1** in chilled isopropylamine afforded a red-brown precipitate, [Sm^{II}]**1**. Vapor diffusion of tetrahydrofuran into a solution of [Sm^{II}]**1** in acetonitrile produced red crystals of [Sm^{II}]**1** that were suitable for X-ray crystallography. [Sm^{II}]**1** is nine coordinate (Figure 1, Figure S2) and adopts a capped cubic geometry, as determined by SHAPE analysis (Figure S5).⁴⁴ One Sm–N^{cap} distance in [Sm^{II}]**1** is slightly elongated [2.934(6) Å] relative to the other [2.904(6) Å], placing Sm^{II} slightly off-center inside the cavity of **1**. The Sm–N^{arm} distances vary from 2.710(5) to 2.802(6) Å with an average of 2.765 Å. The Sm–N^{cap} and Sm–N^{arm} distances in [Sm^{II}]**1** are similar to Eu–N^{cap} [2.901(2) and 2.942(2) Å] and Eu–N^{arm} distances [2.702(2)–2.807(2) Å] of [Eu^{II}]**1**,³⁴ consistent with the similarity of ionic radius between Sm^{II} and Eu^{II}.⁴⁵ The Sm–I bond length [3.6397(5) Å] in [Sm^{II}]**1** is also similar to the Eu–I bond length [3.6300(6) Å] in [Eu^{II}]**1**.³⁴ Sm^{II} is off-center in **1** by 0.030 Å, similar to Eu^{II} in [Eu^{II}]**1** that is off-center by 0.041 Å.³⁴ In contrast, Yb^{II} in [Yb^{II}]**1** is centered inside **1**, with Yb–N^{cap} (both 2.719 Å) and Yb–N^{arm} (all 2.593 Å)²⁸ distances that are shorter than Ln–N distances in both [Sm^{II}]**1** and [Eu^{II}]**1**.³⁴ The differences in bond lengths are consistent with Ln^{II} ion contraction across the series from Sm to Yb.⁴⁵ Overall, Yb^{II} coordinates more uniformly to **1** than both

^a Department of Chemistry, Wayne State University, 5101 Cass Ave., Detroit, MI 48202, USA. Email: mallen@chem.wayne.edu

^b Lumigen Instrument Center, Wayne State University, 5101 Cass Ave., Detroit, MI 48202, United States.

Electronic Supplementary Information (ESI) available: Experimental procedures, X-ray data for [Sm^{II}]**1** and [Sm^{II}]**2**, and Shape analyses of Sm^{II} in [Sm^{II}]**1** and [Sm^{II}]**2**. See DOI: 10.1039/x0xx00000x

Sm^{II} and Eu^{II}. However, coordination of Yb^{II} to **1** requires shrinking of the cavity of **1** to match the smaller ionic radius of Yb^{II} compared to Eu^{II} and Sm^{II}.

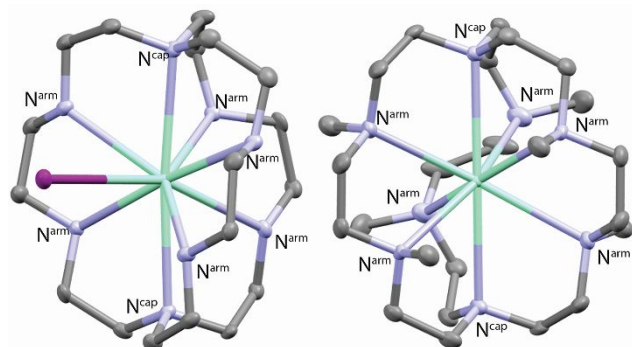


Figure 1. Molecular structures in crystals of (left) [Sm**1**]I and (right) [Sm**2**]₂I₂ with displacement ellipsoids at 50% probability. Hydrogen atoms, solvent molecules, and noncoordinating counter-ions are omitted for clarity. Blue = nitrogen, green = samarium, purple = iodine, and gray = carbon. Crystallographic data for the two structures have been deposited at the Cambridge Crystallographic Data Centre under deposition numbers CCDC 2162698 and 2157499.

We suspect that the observed differences in placement of Yb^{II} inside **1** relative to that of Eu^{II} and Sm^{II} are a result of differences in geometry and coordination number in addition to ionic radii. Thus, to gain insight of the role that coordination number or ionic radii plays on the placement of Ln^{II} ions inside azacryptands, it is crucial that the geometry be held constant. To this end, we synthesized [Sm**2**]₂I₂ because the steric hindrance in **2** limits the coordination number for both Eu^{II} and Yb^{II} to eight and produces Ln^{II}-cryptates that are nearly isostructural. Reaction of SmI₂ and **2** in tetrahydrofuran produced a green precipitate, and subsequent crystallization from acetonitrile/tetrahydrofuran yielded dark-green crystals suitable for X-ray crystallographic analysis. [Sm**2**]₂I₂ is eight coordinate (Figure 1, Figure S4) and the geometry of the Sm^{II} ion in [Sm**2**]₂I₂ is best described as a cube using SHAPE analysis (Table S6).⁴⁴ The orientation of the methyl groups on either side of the cavity of **2** sterically limits the coordination number of Sm^{II} to eight in the solid state even in the presence of a small, linear solvents such as acetonitrile. The Sm–N bond distances in [Sm**2**]₂I₂ display small variations of the Sm–N^{arm} bond lengths between 2.840(5) and 2.872(5) Å with an average length of 2.857(5) Å. The Sm–N^{cap} distances are both 2.931(4) Å.

With the solid-state structural data for [Sm**2**]₂I₂ in hand, we compared bonding trends with nearly isostructural [Eu**2**]₂I₂ and [Yb**2**]₂I₂ cryptates.^{28,34} The Sm–N^{arm} distances in [Sm**2**]₂I₂ are similar to Eu–N^{arm} bond distances of [Eu**2**]₂I₂ (2.832–2.917 Å),³⁴ consistent with the similarity in ionic radius between the two ions.⁴⁵ Interestingly, the Sm–N^{cap} distances are both the same in [Sm**2**]₂I₂, placing Sm^{II} in the center of the cage. In contrast, the Eu–N^{cap} distances (2.974 and 2.821 Å) place Eu^{II} off-center within the cage by 0.153 Å.³⁴ Furthermore, [Yb**2**]₂I₂ shows the greatest preferential binding of Yb^{II} to one side of **2**, as evidenced by Yb–N^{cap} distances of 2.886(7) and 2.719(7) Å and

Yb–N^{arm} bond lengths between 2.687(7) and 3.010(7) Å,²⁸ resulting in Yb^{II} being off-center in **2** by 0.167 Å. Based on these trends in Ln^{II} ion placement inside **2**, smaller Ln^{II} ions are more off-centered in **2** compared to larger Ln^{II} ions. We suspect that this observation is based on better matching between metal ionic radius and ligand cavity size for Sm^{II} and Eu^{II} relative to Yb^{II}. For example, the difference in Yb^{II} placement inside **1** relative to **2** is most likely caused by steric factors that limit the ability of **2** to shrink to match the size of Yb^{II}. The data for Sm^{II} suggest that coordination number is also an important factor to consider when matching ligands to divalent lanthanides.

The preference for Yb^{II} in [Yb**1**]₂ to form an eight-coordinate complex upon chelation by **1** appears to differ from the coordination number of nine observed in analogous complexes with 222.^{28,31} Reported structures of Yb(222)₂I₂, in which the Yb–N^{cap} distances are similar to Yb–N^{cap} distances in [Yb**1**]₂, contain either an inner-sphere iodide or molecule of *N,N*-dimethylformamide.^{28,31} Furthermore, encapsulation of Eu^{II} and Sm^{II} by 222 produces ten-coordinate complexes that have two inner-sphere molecules of *N,N*-dimethylformamide and two outer-sphere iodide counterions.³¹ Additionally, a ten-coordinate Sm^{II}(222) complex that contains two inner-sphere triflates is also known.²⁹ It is thus possible that one source of the observed differences in coordination number between Ln**1**₂ and Ln(222)₂ for Eu^{II} and Sm^{II} is the choice of solvent system employed for crystallization.

With the solid-state data of Sm^{II}-azacryptates in hand, we investigated the effect of steric hindrance on the solution-phase coordination environment of Sm^{II} using UV–visible spectroscopy. UV–visible absorption spectra of SmI₂, [Sm**1**]₂I₂, and [Sm**2**]₂I₂ were recorded in either acetonitrile or *N,N*-dimethylformamide. These two solvents were selected because they dissolve all three complexes of Sm^{II}. The UV–visible spectra of [Sm**1**]₂I₂ in acetonitrile and *N,N*-dimethylformamide show two broad absorptions in the visible spectrum arising from f–d transitions and a shoulder that trails into the UV region (Figure 2). The absorption maxima of [Sm**1**]₂I₂ in acetonitrile (760 nm) and *N,N*-dimethylformamide (750 nm) are red-shifted by 72 and 156 nm, respectively, relative to the absorption maxima of SmI₂ in the same solvents. The observed red-shift in the UV–visible absorption of [Sm**1**]₂I₂ is consistent with the presence of strong-field amine donors lowering the energies of the f–d transitions by increasing 4d orbital splitting.^{34,37} The nearly identical UV–visible spectra of [Sm**1**]₂I₂ in acetonitrile and *N,N*-dimethylformamide suggests similar coordination environments for Sm^{II} in both solvents.

The UV–visible spectra of [Sm**2**]₂I₂ show one broad absorption in the visible region (602 and 580 nm in acetonitrile and *N,N*-dimethylformamide, respectively) and a shoulder (374 nm in both solvents) in the UV region (Figure 2) arising from f–d transitions. These spectra are blue shifted compared to those of [Sm**1**]₂I₂. The blue-shifted absorptions of [Sm**2**]₂I₂ relative to [Sm**1**]₂I₂ are consistent with reported spectra of [Eu**1**]₂I₂ and [Eu**2**]₂I₂ in methanol that show similar trends.^{27–29} Thus, it is likely that the observed blue-shifted UV–visible absorptions of [Sm**2**]₂I₂ are a result of differences in

geometry between $[\text{Sm}1]\text{I}$ and $[\text{Sm}2]\text{I}_2$ in solution, similar to $[\text{Eu}1]\text{I}$ and $[\text{Eu}2]\text{I}_2$.³⁴ Altogether, the UV–visible data suggest similar coordination environments for $[\text{Sm}2]\text{I}_2$ in both solvent media.

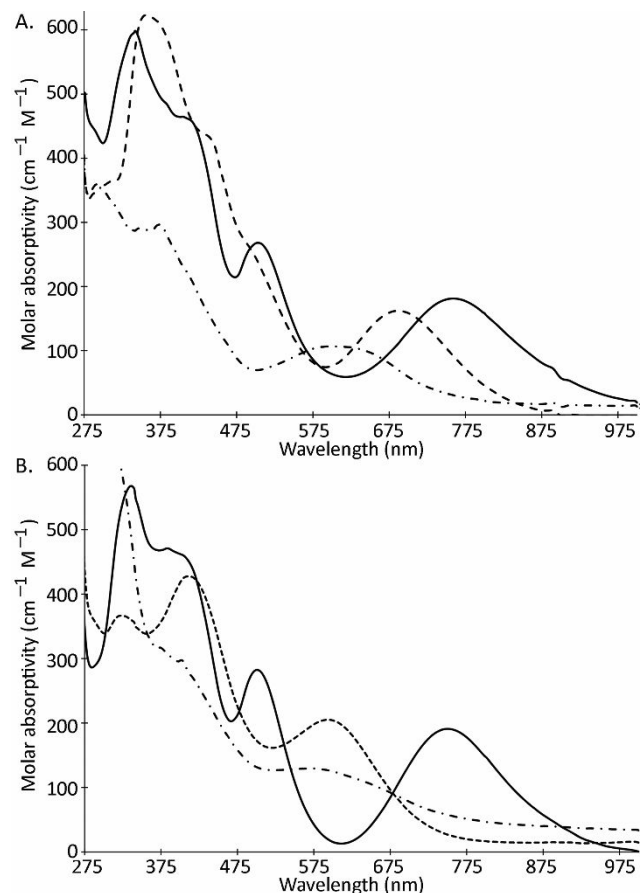


Figure 2. UV–visible spectra of SmI_2 (---), $[\text{Sm}1]\text{I}$ (—), and $[\text{Sm}2]\text{I}_2$ (-·-) in A. acetonitrile ($\text{SmI}_2 = 1.1 \text{ mM}$, $[\text{Sm}1]\text{I} = 0.98 \text{ mM}$, and $[\text{Sm}2]\text{I}_2 = 1.3 \text{ mM}$) and B. *N,N*-dimethylformamide ($\text{SmI}_2 = 0.95 \text{ mM}$, $[\text{Sm}1]\text{I} = 0.99 \text{ mM}$, and $[\text{Sm}2]\text{I}_2 = 0.97 \text{ mM}$) at ambient temperature.

We also compared the ground-state electrochemical potentials of $[\text{Sm}1]\text{I}$ and $[\text{Sm}2]\text{I}_2$ to the reported potentials for $[\text{Yb}1]\text{I}_2$, $[\text{Yb}2]\text{I}_2$, $[\text{Eu}1]\text{I}$, and $[\text{Eu}2]\text{I}_2$. We performed cyclic voltametric experiments with SmI_2 , $[\text{Sm}1]\text{I}$, and $[\text{Sm}2]\text{I}_2$ in *N,N*-dimethylformamide. We selected *N,N*-dimethylformamide to enable direct comparison with reported electrochemical potentials data for $[\text{Yb}1]\text{I}_2$, $[\text{Yb}2]\text{I}_2$, $[\text{Eu}1]\text{I}$, and $[\text{Eu}2]\text{I}_2$ that are all reported in *N,N*-dimethylformamide. The cyclic voltammogram of Sm^{II} -cryptates and SmI_2 show quasi-reversible profiles for SmI_2 and $[\text{Sm}2]\text{I}_2$ centered at -1.58 and -1.62 V vs Ag/AgCl , respectively (Figure 3). $[\text{Sm}1]\text{I}$ has a reversible profile centered at a slightly more positive potential (-1.41 V vs Ag/AgCl) than both SmI_2 and $[\text{Sm}2]\text{I}_2$, consistent with EuI_2 , $[\text{Eu}1]\text{I}$, and $[\text{Eu}2]\text{I}_2$ analogues that display a similar trend.³⁴ The electrochemical potentials of $[\text{Sm}1]\text{I}$ and $[\text{Sm}2]\text{I}_2$ also follow the expected trend in reactivity based on the strength of Lewis basicity of the donor atoms in **1** compared to **2**, similar to trends observed with reported Yb^{II} - and Eu^{II} -containing cryptates.²⁸ Overall, $[\text{Sm}1]\text{I}$ and $[\text{Sm}2]\text{I}_2$ are more reducing than reported analogues containing Yb^{II} and Eu^{II} , and the trends in reducing power are $[\text{Sm}1]\text{I} > [\text{Yb}1]\text{I}_2 > [\text{Eu}1]\text{I}$ and $[\text{Sm}2]\text{I}_2 > [\text{Yb}2]\text{I}_2 > [\text{Eu}2]\text{I}_2$.^{28,34}

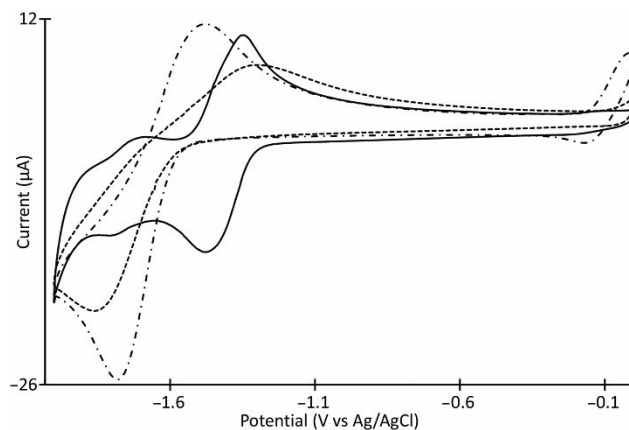


Figure 3. Cyclic voltammogram of SmI_2 (---), $[\text{Sm}1]\text{I}$ (—), and $[\text{Sm}2]\text{I}_2$ (-·-) in *N,N*-dimethylformamide.

In conclusion, we investigated the structural properties of two Sm^{II} -azacryptates in the solid state and in solution. Overall, encapsulation of Sm^{II} in **1** forms a nine-coordinate complex, and chelation of Sm^{II} by **2** produces an eight-coordinate complex. Cyclic voltammetry and UV–visible absorption studies followed the trend in Lewis basicity of donor atoms where the Sm^{II} -cryptate with tertiary-amine donors produces a more reducing complexes than the Sm^{II} -cryptate with secondary amine donors. Our results provide a valuable step forward establishing bonding and reactivity trends across the series of Ln^{II} -cryptates with systematic changes in electronic and steric properties of cryptands.

The authors are grateful to the National Science Foundation for their support (CHE-1564755). X-ray crystallography was performed at the Lumigen Instrument Center, Wayne State University, which is partially supported by the National Institutes of Health (3R01EB027103-02S1).

Author Contributions

Experimental design: SSB, TCJ, and MJA. Data collection: SSB, TCJ, and CLW. Writing and editing: SSB, TCJ, CLW, and MJA.

Conflicts of interest

There are no conflicts to declare.

Notes and references

- 1 N. Kern, M. P. Plesniak, J. J. W. McDouall and D. J. Procter, *Nat. Chem.*, 2017, **9**, 1198.
- 2 J. Li, L. Wang, Z. Zhao, B. Sun, G. Zhan, H. Liu, Z. Bian and Z. Liu, *Nat. Commun.*, 2020, **11**, 5218.
- 3 C. A. Gould, K. R. McClain, D. Reta, J. G. C. Kragsskow, D. A. Marchiori, E. Lachman, E. S. Choi, J. G. Analytis, R. D. Britt, N. F. Chilton, B. G. Harvey and J. R. Long, *Science*, 2022, **375**, 198.
- 4 S. Maity and R. A. Flowers, II, *J. Am. Chem. Soc.*, 2019, **141**, 3207.

- 5 A. Ramírez-Solís, C. O. Bartulovich, T. V. Chciuk, J. Hernández-Cobos, H. Saint-Martin, L. Maron, W. R. Anderson, Jr., A. M. Li and R. A. Flowers, II, *J. Am. Chem. Soc.*, 2018, **140**, 16731.
- 6 C. A. Gould, K. R. McClain, J. M. Yu, T. J. Groshens, F. Furche, B. G. Harvey and J. R. Long, *J. Am. Chem. Soc.*, 2019, **141**, 12967.
- 7 M. Xémard, M. Cordier, F. Molton, C. Duboc, B. L. Guennic, O. Maury, O. Cadour and G. Nocton, *Inorg. Chem.*, 2019, **58**, 2872.
- 8 H. Qi, Z. Zhao, G. Zhan, B. Sun, W. Yan, C. Wang, L. Wang, Z. Liu, Z. Bian and C. Huang, *Inorg. Chem. Front.*, 2020, **7**, 4593.
- 9 S. Agasti, N. A. Beattie, J. J. W. McDouall and D. J. Procter, *J. Am. Chem. Soc.*, 2021, **143**, 3655.
- 10 D. N. Huh, J. P. Bruce, S. G. Balasubramani, S. R. Ciccone, F. Furche, J. C. Hemminger and W. J. Evans, *J. Am. Chem. Soc.*, 2021, **143**, 16610.
- 11 T. N. Poe, S. Molinari, S. Justiniano, G. M. McLeod and T. E. Albrecht-Schönzart, *Cryst. Growth Des.*, 2022, **22**, 842.
- 12 A. Ramírez-Solís, N. G. Boekell, C. I. León-Pimentel, H. Saint-Martin, C. O. Bartulovich and R. Flowers, II, *J. Org. Chem.*, 2022, **87**, 1689.
- 13 R. M. Diaz-Rodriguez, D. A. Gálico, D. Chartrand, E. A. Suturina and M. Murugesu, *J. Am. Chem. Soc.*, 2022, **144**, 912.
- 14 T. V. Chciuk, W. R. Anderson, Jr. and R. A. Flowers, II, *J. Am. Chem. Soc.*, 2018, **140**, 15342.
- 15 S. A. Moehring and W. J. Evans, *Organometallics*, 2020, **39**, 1187.
- 16 A. N. Seilkhov, I. V. Lapshin, A. V. Cherkasov, G. K. Fukin and A. A. Trifonov, *Organometallics*, 2021, **40**, 3042.
- 17 H. Li, Y. Hou, C. Liu, Z. Lai, L. Ning, R. Szostak, M. Szostak and J. An, *Org. Lett.*, 2020, **22**, 1249.
- 18 S. De and S. Hoz, *J. Org. Chem.*, 2021, **86**, 10861.
- 19 D. I. Galimov, S. M. Yakupova and R. G. Bulgakov, *J. Photochem. Photobiol., A*, 2022, **425**, 113711.
- 20 D. I. Galimov, S. M. Yakupova, K. S. Vasilyuk and R. G. Bulgakov, *J. Photochem. Photobiol., A*, 2021, **418**, 113430.
- 21 D. I. Galimov, S. M. Yakupova, K. S. Vasilyuk, D. Sh. Sabirov and R. G. Bulgakov, *J. Photochem. Photobiol., A*, 2020, **403**, 112839.
- 22 D. I. Galimov, S. M. Yakupova, K. S. Vasilyuk and R. G. Bulgakov, *J. Photochem. Photobiol., A*, 2020, **397**, 112587.
- 23 C. N. Rao and H.-U. Reissig, *Eur. J. Org. Chem.*, 2021, 6392.
- 24 S. De, H. E. Gottlieb and S. Hoz, *Chem. Eur. J.*, 2020, **26**, 6846.
- 25 N. Schwarz, X. Sun, R. Yadav, R. Köppe, T. Simler and P. W. Roesky, *Chem. Eur. J.*, 2021, **27**, 12857.
- 26 T. N. Poe, M. J. Beltrán-Leiva, C. Celis-Barros, W. L. Nelson, J. M. Sperling, R. E. Baumbach, H. Ramanantoanina, M. Speldrich and T. E. Albrecht-Schönzart, *Inorg. Chem.*, 2021, **60**, 7815.
- 27 C. U. Lenora, R. J. Staples and M. J. Allen, *Inorg. Chem.*, 2020, **59**, 86.
- 28 T. C. Jenks, A. N. W. Kuda-Wedagedara, M. D. Bailey, C. L. Ward and M. J. Allen, *Inorg. Chem.*, 2020, **59**, 2613.
- 29 D. N. Huh, S. R. Ciccone, S. Bekoe, S. Roy, J. W. Ziller, F. Furche and W. J. Evans, *Angew. Chem. Int. Ed.*, 2020, **59**, 2.
- 30 M. L. Marsh, F. D. White, D. S. Meeker, C. D. McKinley, D. Dan and T. E. Albrecht-Schmitt, *Inorg. Chem.*, 2019, **58**, 9602.
- 31 D. N. Huh, J. W. Ziller and W. J. Evans, *Inorg. Chem.*, 2019, **58**, 9613.
- 32 A. N. W. Kuda-Wedagedara, C. Wang, P. D. Martin and M. J. Allen, *J. Am. Chem. Soc.*, 2015, **137**, 4960.
- 33 G.-X. Jin, M. D. Bailey and M. J. Allen, *Inorg. Chem.*, 2016, **55**, 9085.
- 34 T. C. Jenks, M. D. Bailey, B. A. Corbin, A. N. W. Kuda-Wedagedara, P. D. Martin, H. B. Schlegel, F. A. Rabuffetti and M. J. Allen, *Chem. Commun.*, 2018, **54**, 4545.
- 35 T. C. Jenks, M. D. Bailey, J. L. Hovey, S. Fernando, G. Basnayake, M. E. Cross, W. Li and M. J. Allen, *Chem. Sci.*, 2018, **9**, 1273.
- 36 L. A. Basal, A. B. Kajjam, M. D. Bailey and M. J. Allen, *Inorg. Chem.*, 2020, **59**, 9476.
- 37 B. A. Corbin, J. L. Hovey, B. Thapa, H. B. Schlegel and M. J. Allen, *J. Organomet. Chem.*, 2018, **857**, 88.
- 38 E. L. Yee, O. A. Gansow and M. J. Weaver, *J. Am. Chem. Soc.*, 1980, **102**, 2278.
- 39 R. M. Scarborough, Jr. and A. B. Smith, III, *J. Am. Chem. Soc.*, 1977, **99**, 7088.
- 40 N. Sabbatini, M. Ciano, S. Dellonte, A. Bonazzi, F. Bolletta and V. Balzani, *J. Phys. Chem.*, 1984, **88**, 1534.
- 41 L. Burai, É. Tóth, G. Moreau, A. Sour, R. Scopelliti and A. E. Merbach, *Chem. Eur. J.*, 2003, **9**, 1394.
- 42 N.-D. H. Gamage, Y. Mei, J. Garcia and M. J. Allen, *Angew. Chem. Int. Ed.*, 2010, **49**, 8923.
- 43 L. A. Ekanger, L. A. Polin, Y. Shen, E. M. Haacke, P. D. Martin and M. J. Allen, *Angew. Chem.*, 2015, **127**, 14606.
- 44 M. Llunell, D. Casanova, J. Cirera, P. Alemany and S. Alvarez, SHAPE, version 2.1, Barcelona, Spain, 2013.
- 45 M. Szostak and D. J. Procter, *Angew. Chem. Int. Ed.*, 2012, **51**, 9238.